Edge-localized states in quantum one-dimensional lattices

Ricardo A. Pinto, Masudul Haque, and Sergej Flach
Max-Planck-Institut für Physik komplexer Systeme, Nöthnitzer Str. 38, 01187 Dresden, Germany
(Received 3 March 2009; published 26 May 2009)

In one-dimensional quantum lattice models with open boundaries, we find and study localization at the lattice edge. We show that edge-localized eigenstates can be found in both bosonic and fermionic systems, specifically, in the Bose-Hubbard model with on-site interactions and in the spinless fermion model with nearest-neighbor interactions. We characterize the localization through spectral studies via numerical diagonalization and perturbation theory through considerations of the eigenfunctions and through the study of explicit time evolution. We concentrate on few-particle systems, showing how more complicated edge states appear as the number of particles is increased.

DOI: 10.1103/PhysRevA.79.052118 PACS number(s): 03.65.Ge, 05.30.−d, 68.65.−k, 71.10.Fd

I. INTRODUCTION

Experimental techniques in the fields of mesoscopics and ultracold atoms have advanced to the point where it is feasible to explore the physics of few-boson and few-fermion systems, in particular in lattice systems which have traditionally been the basis for many-particle physics studies. The study of a few quantum particles in lattice situations provides surprises and unexpected phenomena quite distinct from issues in bulk condensed-matter physics, whose focus is on many-particle ground states, and from atomic or optical physics, where lattice systems are not very common. For example, a recent experiment has explored repulsive binding of boson pairs in a one-dimensional optical lattice [1]. This is therefore the appropriate time to investigate further intricate and nonintuitive phenomena involving a few quantum particles in lattice systems. In this paper, we consider interacting bosons or fermions in one-dimensional finite lattices and present studies of *localization* at the lattice edge. We characterize the edge-localized states and distinguish them from bound nonlocalized states through analyses of the energy spectrum and band structure, density profiles of eigenstates, and dynamics.

For bosons, we use the well-known Bose-Hubbard model [2], which has attracted a great deal of attention in the last decade due to its relevance to describing laser-cooled bosonic atoms subjected to an optical-lattice potential [3,4]. Localization in the Bose-Hubbard model is of particular interest because its large-boson limit can for many purposes be approximated by the discrete nonlinear Schrödinger (DNLS) equation, which displays a host of localization phenomena. Nonlinearity allows time-periodic and spatially localized solutions of the DNLS (and other lattice nonlinear differential equations) known as *intrinsic localized modes* or *discrete breathers* [5–9]. More relevant to the present work, the DNLS on finite lattices also possesses edge-localized modes, sometimes called discrete surface solitons [10–12]. It is therefore expected that the large-boson limit of the open-boundary Bose-Hubbard model will possess eigenstates in which the bosons are localized at the edge. In this paper, we pose the edge-localization question in the extreme opposite limit of a *few* quantum particles, where the mean-field approximation (DNLS equation) cannot *a priori* be expected to provide the correct intuition. The answer turns out to be subtle—this phenomenon is not present for the case of two particles but appears when the particle number is three or more, as follows from numerical studies in Ref. [13].

Remarkably, we find that the phenomenon is not restricted to bosons but also happens in other quantum lattice models. For example, the spinless fermion model with nearest-neighbor interactions, sometimes known as the t-V model, has similar behavior, i.e., it possesses no edge states with two fermions, but does have such localized eigenstates with three fermions. Since this model does not allow multiple occupancies, localization in this case refers to a sequence of neighboring sites being occupied rather than all the particles clustered in one site as in the case of bosons. Although the current work will focus on the two models mentioned above, our finding indicates that edge localization may well be a generic phenomenon in quantum finite lattice systems.

Localization in quantum models generally does not appear in simple Hamiltonians, but instead it requires disorder [14] or impurities, breaking the translation invariance. (This is in contrast to lattice differential equations, e.g., the DNLS equation, where the interplay of nonlinearity and spatial discreteness is sufficient to create localization.) It is therefore of significant theoretical interest to explore the simple mechanism for quantum localization that is studied here, requiring only open-boundary conditions in an interacting lattice Hamiltonian. We also note that localization due to impurities or disorder is generally a single-particle effect, while the mechanism we present is a *collective* phenomenon since it requires at least three particles.

While we focus on small numbers of bosons or fermions, the basic message is that edge states exist for any number of particles larger than two. We give an explanation based on perturbation theory. We also provide some hints toward the many-particle situation by showing that the four-boson case has an additional type of edge-localized eigenstate in addition to the obvious generalization.

Model Hamiltonians. We consider one-dimensional lattices with L sites subject to open-boundary conditions. The Bose-Hubbard model Hamiltonian is

$$\hat{H}_{\mathrm{BH}} = -\frac{\gamma}{2}\sum_{j=1}^{L} \hat{a}_j^\dagger \hat{a}_j^\dagger \hat{a}_j \hat{a}_j - t\sum_{j=1}^{L-1} (\hat{a}_j^\dagger \hat{a}_{j+1} + \hat{a}_{j+1}^\dagger \hat{a}_j). \quad (1)$$

Here $\hat{a}$ and $\hat{a}^\dagger$ are the second-quantized bosonic operators. The first and second terms describe, respectively, on-site attractive ($\gamma > 0$) interactions and nearest-neighbor hopping. The edge-localization physics is almost unchanged in the case of repulsive interactions.

The model for spinless fermions is described by

$$\hat{H}_{\mathrm{sf}} = V\sum_{j=1}^{L-1} \hat{c}_j^\dagger \hat{c}_{j+1}^\dagger \hat{c}_{j+1} \hat{c}_j - t\sum_{j=1}^{L-1} (\hat{c}_j^\dagger \hat{c}_{j+1} + \hat{c}_{j+1}^\dagger \hat{c}), \quad (2)$$

where V is the (repulsive) nearest-neighbor interaction strength and $\hat{c}_j$ and $\hat{c}_j^\dagger$ are the fermionic creation and annihilation operators.

Units. We will use the same arbitrary units of energy to express values of t, γ, V, and energy eigenvalues.

II. BOSE-HUBBARD CHAIN WITH TWO AND THREE BOSONS

We will first describe the cases of two bosons and of three bosons in the Bose-Hubbard chain and show how the two situations differ by virtue of the latter having edge states. Some of the physics described in this section appears in Ref. [13].

A. Strong interactions

We first focus on large values of γ, which is the most relevant parameter regime for localization physics. The Hilbert space size (number of basis states) for n bosons in $L > n$ sites is $d_n = \binom{L+n-1}{n}$; in particular $d_2 = L(L+1)/2$ and $d_3 = L(L+1)(L+2)/6$. Figure 1 displays spectral properties and band structure, i.e., the distribution of the d_n eigenenergies. We label the eigenstates from low to high energies with the label ν running from 1 to d_n.

The most prominent feature of the large-γ spectrum is the band structure. For the n-boson system there are $p(n)$ bands, where $p(n)$ is the number of integer partitions of n. In the two-boson case [Figs. 1(a) and 1(c)], there are two bands. In the upper band around zero energy, the dominant contributions come from configurations where the bosons do not share the same site. The lower band contains the L two-boson bound states, dominated by linear combinations of configurations where the bosons sit on the same site. These are the quantum analogs of classical discrete breather solutions. This band is thus called the quantum breather band or the soliton band [15]. In these states, the separation probability of the bosons decays exponentially with distance [16–18].

In the three-boson case [Figs. 1(b) and 1(d)], the spectrum contains three energy bands. The lowest-energy band is formed by the L three-boson bound states (three-boson breather band), where there is a high probability of finding the three bosons at the same lattice site. The second band from below is formed by $L(L-1)$ "2+1-boson states," where there is a high probability of finding two bosons at the same lattice site with the third boson elsewhere. Finally, the third

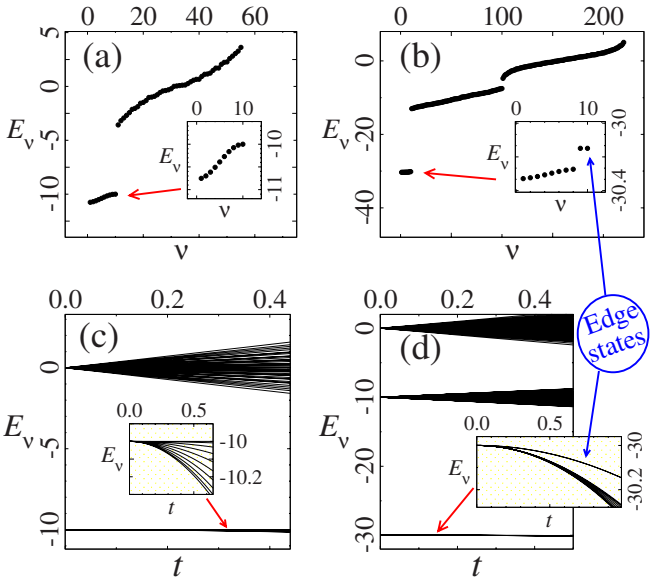

FIG. 1. (Color online) Energy spectrum of ten-site Bose-Hubbard chain with $\gamma = 10$. Left panels (a) and (c) show the case of two bosons ($n=2$), right panels (b) and (d) show $n=3$. Top panels (a) and (b) plot-ordered energies against eigenvalue index ν, for fixed hopping parameter $t=1$. Lower panels (c) and (d) plot energies against hopping strength t. Insets focus on the lowest (breather) band, showing that two edge-localized states separate out [(b) and (d)] for three bosons but not [(a) and (c)] for two bosons. Here t, γ, and E_ν are expressed in the same arbitrary energy units.

band is the three-boson continuum, whose $L(L-1)(L-2)/6$ eigenstates are characterized by having the three bosons in different sites.

The edge states can be identified by zooming onto the three-boson bound state band [insets of Figs. 1(b) and 1(d)]. We note that two states stand out from the rest of the band, with larger splitting. These are the edge states, as we demonstrate further below. Because of reflection symmetry, the dominant contributors to the two eigenstates are not the left-edge and right-edge states ($|E_l\rangle = |3000\ldots\rangle$ and $|E_r\rangle = |\ldots 0003\rangle$) directly. Instead, the eigenstates are dominated by the linear combinations $\frac{1}{\sqrt{2}}(|E_l\rangle \pm |E_r\rangle)$. The remaining $(L-2)$ eigenstates of the breather band are dominated by linear combinations of the remaining $(L-2)$ three-boson bound state configurations, $|03000\ldots\rangle$, $|00300\ldots\rangle$, …, $|\ldots 0030\rangle$. These $(L-2)$ states do not mix with the two edge states because of the energy splitting. Note that the energy-separated edge-localized states are not present in the two-boson case [insets of Figs. 1(a) and 1(c)].

To see the localized nature of the edge states, in Fig. 2 we plot density profiles (site occupancies), i.e., expectation values of boson number at each lattice site, $\langle n_j \rangle_\nu = \langle \chi_\nu | \hat{a}_j^\dagger \hat{a}_j | \chi_\nu \rangle$, $|\chi_\nu\rangle$ being an eigenstate. Figure 2 shows $\langle n_j \rangle$ against j for the edge states, and also for two other eigenstates (nonedge breather states) for comparison. We see that the edge states are exponentially localized at the edges of the lattice, as seen through the linear behavior of $\ln\langle n_j \rangle$ in the inset.

The localization is further demonstrated through the scaling of the largest site occupancies, $\max\langle n_j \rangle$, with system size L (Fig. 3). For eigenstates that are localized, this quantity

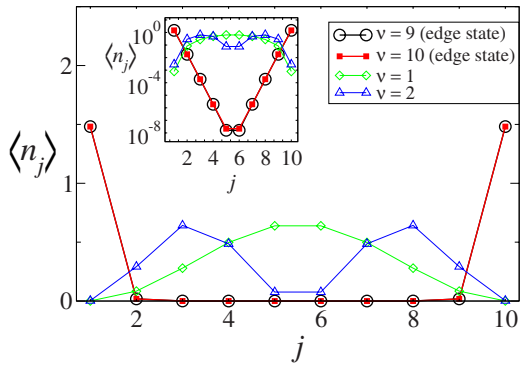

FIG. 2. (Color online) Spatial profile of site occupancies for several eigenstates of the three-boson Bose-Hubbard chain. Inset shows the same plot in semilogarithmic scale, the linear behavior indicating exponential localization in the edge states. Here $L=10$ and $\gamma=10t$.

will be independent of the system size, whereas for extended states it should be a linear function of $1/L$ because the bosons are spread across L sites in extended states. In the two-bosons case [Fig. 3(a)] all eigenstates are extended, thus $\max\langle n_j\rangle$ depends linearly on $1/L$ for all of them. In Fig. 3(b) for three bosons, most states also have $\max\langle n_j\rangle$ varying as $\sim L^{-1}$, except for two states for which $\max\langle n_j\rangle$ are independent of L. This flat set of points in Fig. 3(b) clearly illustrates the localization phenomenon.

We have described the spectrum for the attractive Bose-Hubbard model. The spectrum for the repulsive case ($\gamma<0$) is obtained simply by inverting the energies ($E_\nu \rightarrow -E_\nu$). The eigenfunction characteristics described in Figs. 2 and 3 are identical in the repulsive case.

B. Weak interactions

It is natural to ask whether the edge-localization survives for weaker interactions. In particular, for three bosons and

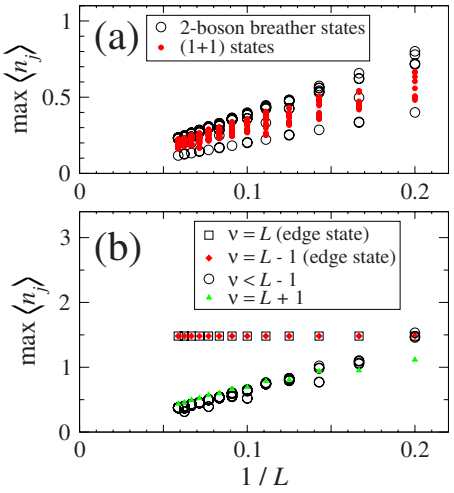

FIG. 3. (Color online) Size-dependence of $\max\langle n_j\rangle$ for (a) all eigenstates of the two-boson Bose-Hubbard chain and (b) several eigenstates of the three-boson Bose-Hubbard chain labeled by ν. Here $\gamma=10t$, and L goes from $L=5$ to $L=17$.

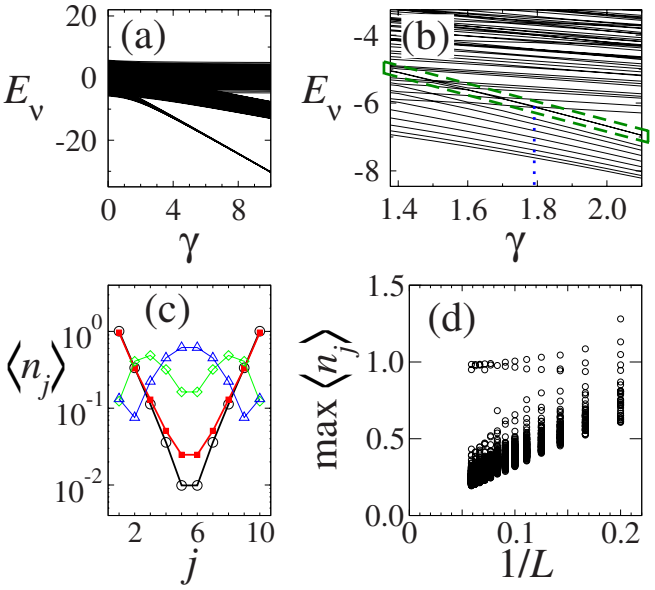

FIG. 4. (Color online) Spectrum and density profiles at smaller interactions for three-boson system in ten sites ($t=1$). Here t, γ, and E_ν are expressed in the same arbitrary units. (a) The bands merge at small enough γ. (b) For this system the breather band loses its identity around $\gamma\sim 1.8$. We follow the edge-localized states at smaller γ; shown surrounded by a thick-lined dashed polygon. At smaller γ, the $\nu=(L-1)$ and $\nu=L$ states are no longer the edge states. (c) Site occupancies at $\gamma=1.4$. The almost exponentially localized curves are for the edge states, and the two nonlocalized curves are the $\nu=(L-1)$ and $\nu=L$ states, which are no longer the edge-localized states. (d) Size-dependence of $\max\langle n_j\rangle$.

$\gamma\lesssim 2$, the breather band merges with the 2+1 band [Fig. 4(a)]. One might speculate that there might be a sharply defined value of γ below which there is no localization at the edges.

We address this question by following the two edge states adiabatically to lower values of γ, for three bosons in 10 sites, as shown in Fig. 4(b). Note that, after the breather band has merged, the $\nu=L-1$ and $\nu=L$ states are no longer the edge states. In Fig. 4(c) we plot the spatial density profiles of the two edge states, as well as the nonlocalized $\nu=L-1$ and $\nu=L$ states. Figure 4(d) shows the size dependence of $\max\langle n_j\rangle$. The localization is weaker than in the large-γ situation ($\max\langle n_j\rangle$ is less than 1.5 and the exponential decay is imperfect), but it is still present. Thus the localization phenomenon does not completely disappear at some sharp value of γ, at least for small ($L\sim 10$) lattice sizes.

III. PERTURBATION THEORY

The basic explanation for the edge-localization phenomenon is that the edge states split off from the rest of the breather band for three or more particles. We will now explain this energy splitting through perturbative calculations in the hopping parameter. It is helpful to introduce an effective single-particle model, which contains only the parts of the Hilbert space relevant for this analysis.

For the two-boson case, we keep the L breather-band states, each corresponding to both bosons in the same site.

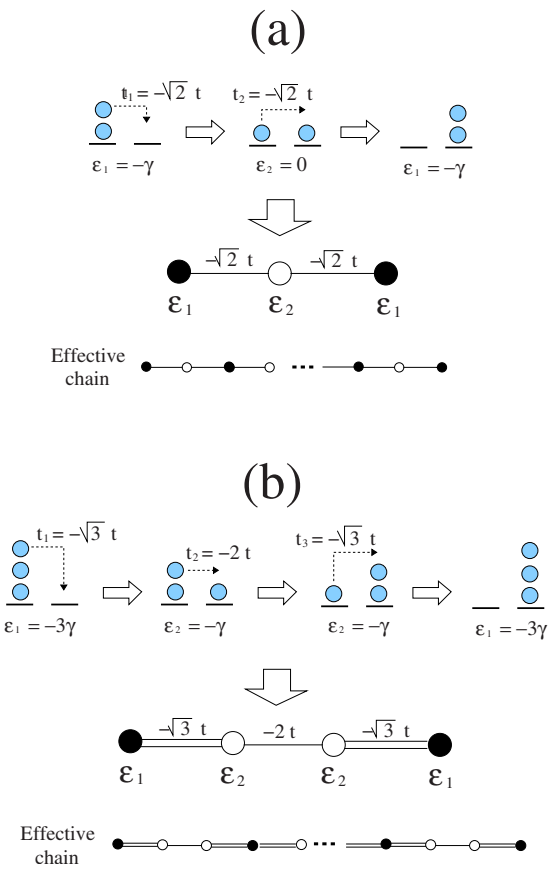

FIG. 5. (Color online) Construction of the effective single-particle chain for the Bose-Hubbard model with (a) two bosons and (b) three bosons. The sequence of hops of the two bosons (gray circles), initially at the same lattice site, are shown with the corresponding values of the matrix element of the Bose-Hubbard Hamiltonian. The energies ε_1 and ε_2 of the states after each hop are also shown. The resulting effective single-particle chain is shown in the lower part of the figures.

We keep only those states of the continuum that are necessary as intermediate configurations to go from one breather state to another, i.e., states where the two bosons are in neighboring sites. In Fig. 5(a), the two-boson states are shown with filled circles and the intermediate 1+1-boson states as open circles; together, they form the single-particle effective tight-binding chain. This effective chain has two different on-site energies $\varepsilon_1=-\gamma$ and $\varepsilon_2=0$ alternating along the chain [Fig. 5(a)]. The effective hopping strength is $\sqrt{2}t$ since the hopping is always from or to a doubly occupied site in the original model. For a fixed size L of the Bose-Hubbard chain, the size of the effective single-particle chain, i.e., the number of states retained from the original Hilbert space, is $L+(L-1)=(2L-1)$.

Similarly, for the three-boson case we retain the L breather-band states, and only those states of the $(2+1)$ band that are necessary as intermediate configurations to go from one breather state to another, i.e., states where the two bosons and the lone boson are in neighboring sites. The single-particle chain now has two on-site energies $\varepsilon_1=-3\gamma$ and $\varepsilon_2=-\gamma$, and two hoppings $t_1=\sqrt{3}t$ and $t_2=2t$. They form a chain of basis three per unit cell [Fig. 5(b)].

Degeneracy splitting. At zero hopping ($t=0$) or infinite interaction, all bands, including the breather band which we are particularly interested in, are perfectly degenerate. We analyze the splitting of the breather-band spectrum perturbatively in the hopping parameter t. The Hamiltonian is $\hat{H}=\hat{H}_0+t\hat{H}_1$, where $\hat{H}_0$ is the interaction term. Since the relevant states of the Hilbert space are arranged along a single chain in the single-particle effective picture, we can use the position on the effective chain as a label for the relevant states. For example, for the two-boson system,

$$\hat{H}_0 = \sum_{m=1}^{L} \varepsilon_1 |2m-1\rangle\langle 2m-1| + \sum_{m=1}^{L-1} \varepsilon_2 |2m\rangle\langle 2m|, \qquad (3)$$

while the perturbation $\hat{H}_1$ contains hopping terms such as $|2m\rangle\langle 2m+1|$.

For two bosons, the lowest order at which the perturbation has nontrivial effects is $O(t^2)$. The hopping perturbation at this order already connects the states of the ground-state manifold to each other, leading to a complete lifting of the degeneracy, so that the nondegenerate breather band emerges. The split energies are approximately $E_{2m-1} \approx -\gamma - 4t^2(1+\cos k_m)/\gamma$.

For the three-boson case, one can carry out a similar analysis. The crucial difference is that, at second order in t, the lowest-manifold states are each connected to themselves and thus receive an energy shift but are not connected to other states within the manifold, and therefore the degeneracy is not lifted. The energy shifts are different for the edge and nonedge states because there is a single path for an edge state to couple to itself via two hopping events, while each nonedge state has two such paths. This is visually obvious through hopping events in real space in our effective single-particle chain (Fig. 5). The shifts at second order are

$$E_{\text{edge}} = -3\gamma - \frac{3}{2\gamma}t^2,$$

$$E_{\text{nonedge}} = -3\gamma - \frac{3}{\gamma}t^2. \qquad (4)$$

At the next order (t^3) the degeneracy of the nonedge states is lifted since three hopping events are required to connect two distinct members of the breather manifold. The degeneracy of the two edge states is only broken at much higher order.

This analysis reveals the reason for the separating out of the edge states from the rest of the breather band. The energy shift of the edge states happens at lower order in the hopping than the order at which the degeneracy of the breather band is lifted. Therefore the edge states are robustly separated out for large interactions.

Figure 6 plots the second-order perturbative results for the breather-band energies, comparing with the exact energies computed numerically. The splitting of the edge-localized states from the rest of the band, which is the essential issue here, is well described by perturbation theory. The degeneracy lifting of the nonedge breather states is not captured in the second-order expressions.

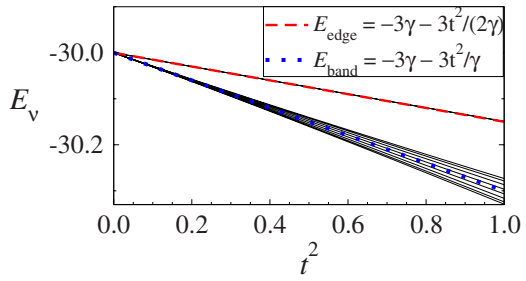

FIG. 6. (Color online) Energies from second-order perturbation theory (dashed and dotted lines) compared with full spectrum (solid lines), for $\gamma=10$ and $L=10$. Here t, γ, and E_ν are expressed in the same arbitrary units.

IV. FOUR OR MORE BOSONS

Edge-localized eigenstates also exist in Bose-Hubbard chains with $n \geq 3$ bosons; the perturbative argument we provided for three bosons can readily be extended to the general case. At strong interactions, the lowest band is the breather band with n-boson bound states. At $t=0$, this band is collapsed as the L-fold degenerate ground state. For $t \neq 0$ the degeneracy is lifted at order $O(t^n)$, but the edge states already have a distinct energy shift at $O(t^2)$, leading to edge localization. As in the $n=3$ case, one can also visualize the perturbative calculation with an effective single-particle model retaining only the relevant basis states. This will now have n-site unit cells, i.e., sites representing breather states separated by $n-1$ sites representing states from other bands.

In addition to the edge-localized states with all n bosons situated at the edge, for $n>3$ the open Bose-Hubbard chain also has edge states with more complicated structure. We demonstrate this for $n=4$ in Fig. 7. Other than the two edge modes on top of the breather band, we see features in the 2+2 band. As in the translation-symmetric case [19], this band has a subband separating out [middle inset in Fig. 7(c)]. This subband of $L-1$ states is characterized by two doubly-occupied sites neighboring each other (2+2 bound states), while the rest of the 2+2 band is dominated by two occupied sites at larger distances from each other. Unlike the translation-symmetric case, however, if one zooms in further onto this subband, two edge-localized states separate out [rightmost inset in Fig. 7(c)]. These edge states have the structure of two bosons at the edge, and the other two at the next-to-edge site. Figures 8(a) and 8(b) show the density profiles of these two types of edge states in the $n=4$ case.

The above results demonstrate the existence of more and more complicated additional edge states as the number of particles is increased.

V. SPINLESS FERMIONS

We now turn to the spinless fermion model described by Hamiltonian (2). Figure 9 displays through numerically calculated spectral properties that in this model, edge states do not exist for the two-fermion case but appear when there are three or more fermions. The situation is thus similar to the Bose-Hubbard model.

We first note that the spectrum of this model contains a breather band as in the Bose-Hubbard model [15]. The Fermi

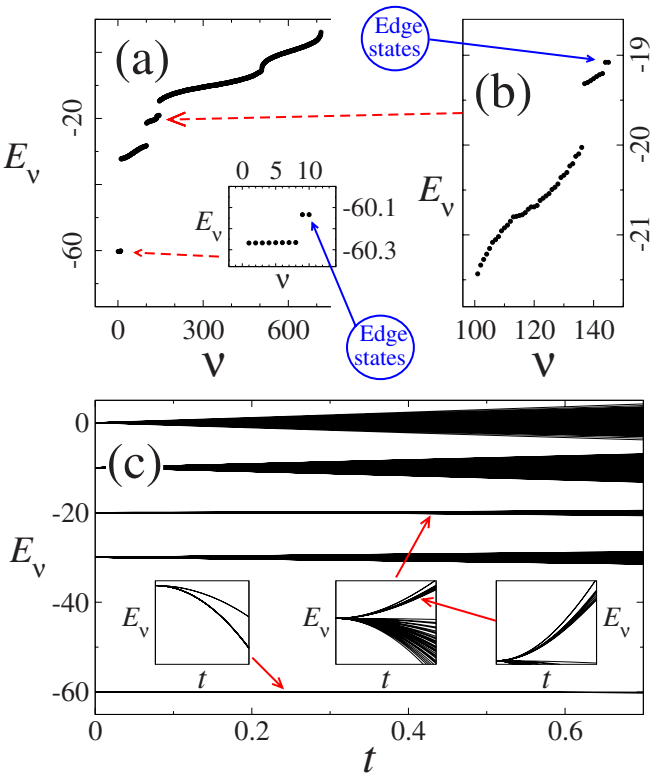

FIG. 7. (Color online) (a) Energy spectrum of the Bose-Hubbard chain with four bosons, plotted against eigenvalue label. The inset zooms onto the breather band, while (b) zooms onto the (2+2)-boson band, as indicated by the dotted red arrows. Here $\gamma=10$, $t=1$, and $L=10$. (c) Spectrum of same chain as a function of the hopping parameter t. The insets focus, from left to right, on the four-boson bound state band, the 2+2-boson band, and the 2+2-boson bound state subband, showing the separation of edge-localized states out of the former and the latter. Here t, γ, and E_ν are expressed in the same arbitrary units.

statistics forbids multiple occupancy of the sites; so the breather modes correspond to all the fermions clustered in a connected segment of the lattice. Since we are using repulsive interactions ($V>0$), the breather band now appears at the top of the spectrum.

The spectral splitting of edge states is analogous to what we have described in the Bose-Hubbard case. For the two-fermion case, the breather band is completely split because the separation for edge and nonedge states all occurs at the same (second) order in t/V. For three or more fermions, however, the two edge states split off from the main band at lower order than the degeneracy-lifting of the rest of the band. As a result, there are now two edge-localized states separated at the bottom of the breather band.

Figure 10 shows density profiles for the edge-localized states as well as some nonlocalized states from the breather band. Each edge state now has a "width" of three sites because of fermionic statistics forbidding double occupancies. Since the two eigenstates are predominantly linear combinations of left-edge $|1110000\ldots\rangle$ and right-edge $|\ldots0000111\rangle$ states, they have occupancies of $n_j \approx 1/2$ at the last three sites of each edge. As in the Bose-Hubbard case, the logarithmic plot makes clear the exponential nature of the local-

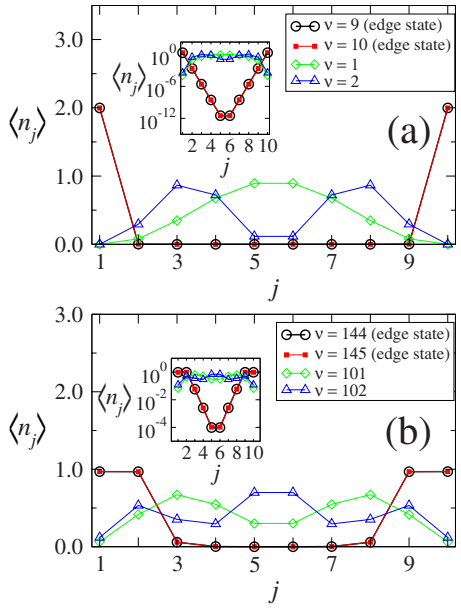

FIG. 8. (Color online) Profile of the site occupancy in the Bose-Hubbard chain with four bosons for four eigenstates in (a) the four-boson bound state band and (b) the 2+2-boson bound state band. The same plots in semilogarithmic scale are shown in the insets, showing exponential localization. Here $L=10$ and $\gamma=10t$.

ization. In this case the exponential decay starts after the third site.

In Fig. 11, we display the robustness of the three-fermion edge states by plotting the size dependence of the maximum site occupancy for a fixed interaction potential. Analogous to the Bose-Hubbard model (Fig. 3), the two-fermion case has

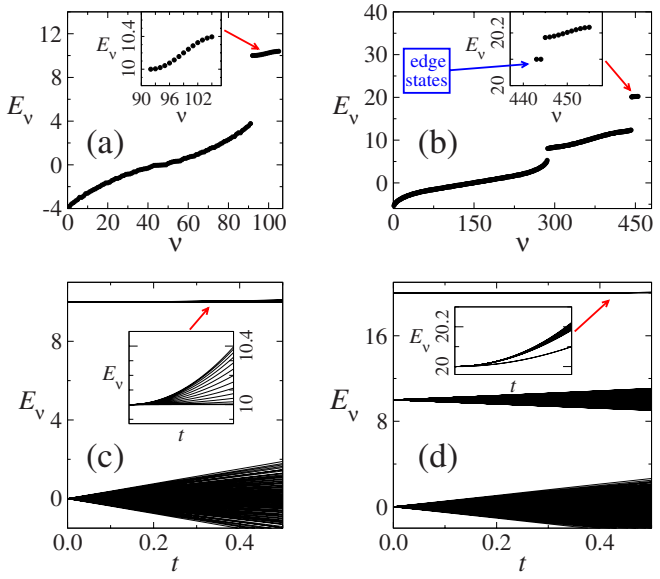

FIG. 9. (Color online) Energy spectrum of the spinless fermion model, for two fermions in left panels (a) and (c) and three fermions in right panels (b) and (d). Here $L=15$, $V=10$. Also, $t=1$ [(a) and (b)] for the top figures. Insets focus on the (topmost) breather band. [(b) and (d)] The three-fermion cases have two states separating from this band; [(a) and (c)] the two-fermion cases do not have this feature. Here t, γ, and E_ν are expressed in the same arbitrary units.

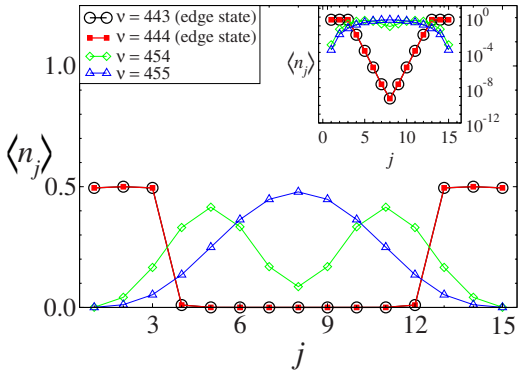

FIG. 10. (Color online) Spatial profile of fermion occupancies, for several eigenstates of the three-fermion model with $L=15$ and $V=10t$. Same plot in semilogarithmic scale is shown in the inset, indicating exponential localization.

$\max\{\langle n_j\rangle_\nu\}$ values all varying as $\sim L^{-1}$, for all states. In the three-fermion case, all eigenstates except two also have linear $1/L$-dependence, while the two exceptions are the edge states for which $\max\{\langle n_j\rangle_\nu\}$ has the constant value of 1/2. This demonstrates, once again, that all states in the two-fermion case are extended in space, while the three-fermion system possesses two localized states.

VI. DYNAMICS (TIME DEPENDENCE)

It is instructive to study the localization phenomenon through explicit time evolution calculations. For the Bose-Hubbard model, some dynamical results have appeared in Ref. [13]. In Fig. 12, we present temporal dynamics results for the spinless-fermion model.

For a three-fermion system in $L=10$ sites, we present the evolution of the occupancies of individual sites, $n_j(t)$, after

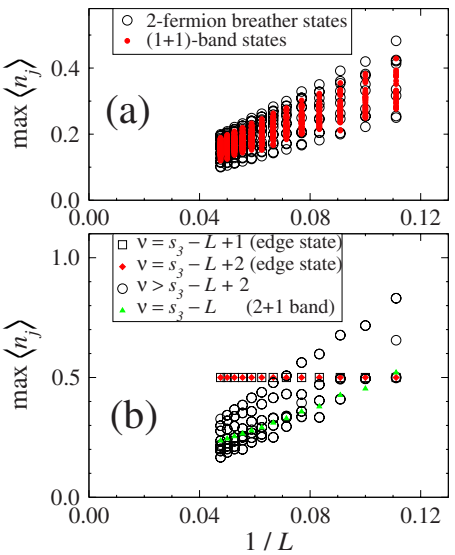

FIG. 11. (Color online) $1/L$-dependence of $\max\langle n_j\rangle$ for (a) all eigenstates of the two-fermion chain and (b) some eigenstates of the three-fermion chain. Here $V=10t$, and L goes from $L=9$ to $L=21$. Here s_3 is the Hilbert space size.

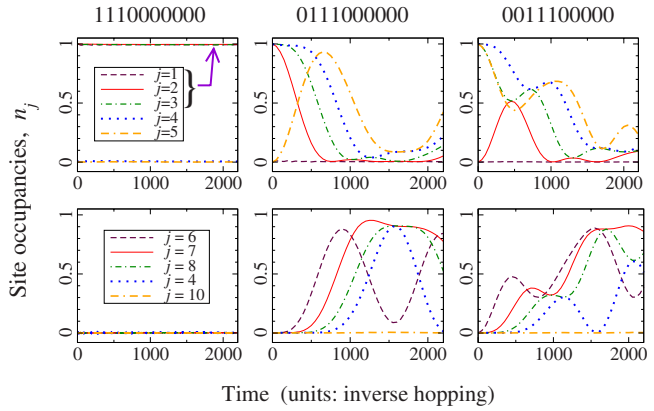

FIG. 12. (Color online) Dynamics of three fermions in ten sites, shown through the evolution of site occupancies n_j. The three different initial conditions are shown on top. In each case, to avoid clutter we split the ten n_j into two groups of five. Thus the left top and left bottom describe two parts of the same evolving chain. Here $V=20$ and $t=1$.

the system is started with the three fermions in consecutive sites. The left panels display the behavior when the fermions in the initial state are concentrated at one edge (the first three sites). There is no appreciable dynamics at the time scales shown, in marked contrast to the cases where the fermions start off at three other consecutive sites (middle panels and right panels). This difference is a dynamical demonstration of the edge-localization phenomenon.

Additional physics can be gleaned from the temporal dynamics shown in Fig. 12. In the cases where we start from three nonedge consecutive sites (center and right panels), the first and last sites are never excited ($n_{j=1}$ and $n_{j=10}$ remain practically zero). This reflects the spectral separation of the edge states, $|e_{\pm}\rangle \approx (|1110000\ldots\rangle \pm |\ldots 0000111\rangle)/\sqrt{2}$, from the rest of the breather band. Since the initial configuration is within the breather band, the dynamics is dominated by this band. Since the edge-localized subspace spanned by the basis $\{|1110000\ldots\rangle, |\ldots 0000111\rangle\}$ is separated from the rest of the breather band, the last and first sites are not excited.

Time scales. Figure 12 highlights dynamics at the scale of hundreds to thousands of t^{-1} units. The reason is that the dominant dynamics for our chosen initial conditions is that within the breather band; hence we are interested in coherent hopping of the three fermions. Such a cooperative hop event of three fermions, from one soliton (neighboring) configuration to the next, involves two intermediate states that are energetically $\sim V$ away, in the $(2+1)$ band. Thus the energy involved is of order t^3/V^2 so that the time scales are $\sim V^2/t^3$. For $V=20$, this leads to the above-mentioned time scales. Performing simulations at other values of V, we have seen that the relevant time scale indeed varies as $\sim V^2$.

There is, of course, additional dynamics at other time scales. Tiny high-frequency wiggles can be seen in our data at scales of $\sim t^{-1}$, representing high-energy interband processes. Also, considering the left panel of Fig. 12, we note that the state $|1110000\ldots\rangle$ is not itself an eigenstate; the true eigenstates are $|e_{\pm}\rangle$. Thus, there will be oscillations involving these two edge states, which is not visible here because the relevant time scales are much higher, and grow exponentially with the chain length.

VII. CONCLUSIONS

In this paper, we have presented a straightforward and natural mechanism for localization in quantum lattice systems, namely, the existence of open boundaries. Our edge localization is a cooperative, as opposed to single-particle phenomenon. We have provided perturbative arguments to explain the energy spectrum structure that lies at the heart of this localization phenomenon thereby also explaining why at least three particles are required for the localization. In addition, we have showed the appearance of richer edge configurations that appear for larger numbers of particles and characterized the energy spectrum and localization through a study of explicit temporal dynamics.

A. Energy scales

At strong interactions, the bands are the most pronounced feature of the energy spectrum. The band energies are set by the interaction strength (U or V). One can then think of finer features of these bands, in various orders of the hopping t. There is always an energy shift at second order in t since a basis state can be connected to itself through two hops. Whenever the degeneracy lifting requires higher than second order in t, we can have subband structures due to differing energy shifts at second order. In the two-boson or two-fermion case, this possibility does not exist. In the three-boson or three-fermion case, only the breather band splits at higher than second order, while the other two bands have degeneracy lifting at linear order. [The linear splitting is manifested in the shapes of the nonbreather bands in Figs. 1(d) and 9(d).] Therefore in the three-particle systems only the breather band can have a subband; this subband turns out to have two members which are edge states.

To rephrase, edge localization from the breather band can be seen as a result of the competition between (a) the distinct energy shifts $\sim t^2/U$ received by the edge states and (b) the degeneracy splitting for which the energy scale is $\sim t^n/U^{n-1}$, for an n-boson system. For $n>3$, analogous energy scale competitions can also play a role in other (multibreather) bands where splitting occurs at larger order, leading to subbands and more complicated edge states. We have illustrated this for $n=4$ in Sec. IV.

Finally, we note that the two edge states separating out from the breather band are themselves very nearly degenerate at strong interactions. This degeneracy gets broken only at much higher order; the relevant energy scale is $U(t/U)^{\beta}$, with $\beta \sim L$ for a chain with L sites.

Interestingly, some of these energy scale issues are manifested *dynamically* in the study of temporal evolution, as discussed in Sec. VI.

B. Possible applications

The edge localization has real-space effects on the dynamics, as revealed by our time evolution calculations (Sec. VI and Fig. 12). This raises the possibility of exploiting these effects for experimental quantum control of bosons or fermions in one-dimensional lattices. If one starts at a breather-band configuration that is not an edge state, the edge modes

will not be excited, and conversely, fermions or bosons populated in an edge configuration remain stable in that configuration for a long time (Fig. 12). One can conceivably use this effect, arising from fine structures in the energy spectrum, to manipulate and select sites for a few-particle lattice system in cold-atom or quantum wire experiments.

C. Open issues

Our work opens up a host of open questions and issues, of which we mention a few. First, our calculations shown in Fig. 4 indicate that for moderate-sized lattices, edge localization persists in some form at weak interactions. The fate of this weak-interaction localization for large lattice sizes remains an unresolved question.

Our work with two separate Hamiltonians results suggest that edge localization is a generic phenomenon for quantum lattice models. Analogous phenomena can possibly be found in other one-dimensional itinerant fermionic and bosonic models. It is obviously of interest to investigate this phenomenon in various other quantum chain models, such as the one-dimensional fermionic Hubbard and extended Hubbard models.

In the discrete nonlinear Schrödinger (DNLS) equation, one can find localized states at all lattice sites, both bulk and edge [11]. In contrast, for three or four bosons we have only found localization of all particles at the edge, even though some of our localized states have a finite width of more than one site. Can the Bose-Hubbard model support solitons some distance away from the edge, perhaps at larger boson numbers?

Since our edge-localized states are quantum analogs of DNLS edge breathers, it is interesting to note that other quantum analogs of DNLS localization have been discussed in the literature [20–23], involving lattice phonons instead of particles with quadratic dispersion as in our case. A thorough comparison with analogous phenomena (or absence thereof) in phonon systems remains an open issue.

It may be interesting to characterize the exponential decay of edge-localized states away from the edges (Figs. 2 and 10), as a function of interaction, particle size, etc. Some results have appeared in Ref. [13].

Finally, since edge-localized classical breathers are known for two-dimensional lattices [24], there is the intriguing possibility of edge states in two-dimensional quantum lattices, which remains unexplored at present.

ACKNOWLEDGMENTS

The authors would like to thank A. Läuchli and Jean Pierre Nguenang for discussions. This work was supported by the ESF network-program AQDJJ.

[1] K. Winkler, G. Thalhammer, F. Lang, R. Grimm, J. Hecker Denschlag, A. J. Daley, A. Kantian, H. P. Büchler, and P. Zoller, Nature (London) **441**, 853 (2006).
[2] M. P. A. Fisher, P. B. Weichman, G. Grinstein, and D. S. Fisher, Phys. Rev. B **40**, 546 (1989).
[3] D. Jaksch, C. Bruder, J. I. Cirac, C. W. Gardiner, and P. Zoller, Phys. Rev. Lett. **81**, 3108 (1998).
[4] M. Greiner, O. Mandel, T. Esslinger, T. W. Hnsch, and I. Bloch, Nature (London) **415**, 39 (2002).
[5] S. Flach and C. R. Willis, Phys. Rep. **295**, 181 (1998); S. Flach and A. V. Gorbach, *ibid.* **467**, 1 (2008).
[6] D. K. Campbell, S. Flach, and Y. S. Kivshar, Phys. Today **57**(1), 43 (2004).
[7] S. Aubry, Physica D **103**, 201 (1997).
[8] A. J. Sievers and J. B. Page, in *Dynamical Properties of Solids VII, Phonon Physics: The Cutting Edge*, edited by G. K. Horton and A. A. Maradudin (Elsevier, Amsterdam, 1995), p. 137.
[9] S. Aubry, Physica D **216**, 1 (2006).
[10] K. G. Makris, S. Suntsov, D. N. Christodoulides, G. I. Stegeman, and A. Hache, Opt. Lett. **30**, 2466 (2005); M. Molina, I. L. Garanovich, A. A. Sukhorukov, and Yu. Kivshar, *ibid.* **31**, 2332 (2006).
[11] M. I. Molina, R. A. Vicencio, and Y. S. Kivshar, Opt. Lett. **31**, 1693 (2006).
[12] S. Suntsov, K. G. Makris, D. N. Christodoulides, G. I. Stegeman, A. Hache, R. Morandotti, H. Yang, G. Salamo, and M. Sorel, Phys. Rev. Lett. **96**, 063901 (2006); E. Smirnov, M. Stepic, C. Ek. Rüter, D. Kip, V. Shandarov, Opt. Lett. **31**, 2338 (2006); C. R. Rosberg, D. N. Neshev, W. Krolikowski, A. Mitchell, R. A. Vicencio, M. I. Molina, and Y. S. Kivshar, Phys. Rev. Lett. **97**, 083901 (2006).
[13] V. Pouthier, Phys. Rev. B **76**, 224302 (2007).
[14] P. W. Anderson, Phys. Rev. **109**, 1492 (1958).
[15] A. C. Scott, J. C. Eilbeck, and H. Gilhøj, Physica D **78**, 194 (1994).
[16] J. C. Eilbeck, in *Localization and Energy Transfer in Nonlinear Systems*, edited by L. Vazquez, R. S. MacKay, and M. P. Zorzano (World Scientific, Singapore, 2003), p. 177.
[17] J. P. Nguenang, R. A. Pinto, and S. Flach, Phys. Rev. B **75**, 214303 (2007).
[18] A. C. Scott, *Nonlinear Science* (Oxford University Press, Oxford, 1999).
[19] J. Dorignac, J. C. Eilbeck, M. Salerno, and A. C. Scott, Phys. Rev. Lett. **93**, 025504 (2004).
[20] W. Z. Wang, J. T. Gammel, A. R. Bishop, and M. I. Salkola, Phys. Rev. Lett. **76**, 3598 (1996).
[21] L. S. Schulman, D. Tolkunov, and E. Mihokova, Phys. Rev. Lett. **96**, 065501 (2006).
[22] V. Pouthier and C. Falvo, Phys. Rev. E **69**, 041906 (2004).
[23] L. S. Schulman, D. Tolkunov, and E. Mihóková, Chem. Phys. **322**, 55 (2006).
[24] R. A. Vicencio, S. Flach, M. I. Molina, and Y. S. Kivshar, Phys. Lett. A **364**, 274 (2007).